Interrupted Self-Organization of SiGe Pyramids

Jean-Noël Aqua,[1,*] Adrien Gouyé,[2] Antoine Ronda,[2] Thomas Frisch,[3] and Isabelle Berbezier[2,†]

[1]*Institut des Nanosciences de Paris, Université Pierre et Marie Curie Paris 6 and CNRS UMR 7588, 4 place Jussieu, 75252 Paris, France*

[2]*Institut Matériaux Microélectronique Nanoscience de Provence, Aix-Marseille Université, UMR CNRS 6242, 13997 Marseille, France*

[3]*Institut Non Linaire de Nice, Université de Nice Sophia Antipolis, UMR CNRS 7335, 1361 routes des Lucioles, 06560 Valbonne, France*

(Received 27 August 2012; published 26 February 2013)

We investigate the morphological evolution of SiGe quantum dots deposited on Si(100) during long-time annealing. At low strain, the dots' self-organization begins by an instability and interrupts when (105) pyramids form. This evolution and the resulting island density are quantified by molecular-beam epitaxy. A kinetic model accounting for elasticity, wetting, and anisotropy is shown to reproduce well the experimental findings with appropriate wetting parameters. In this nucleationless regime, a mean-field kinetic analysis explains the existence of nearly stationary states by the vanishing of the coarsening driving force. The island size distribution follows in both experiments and theory the scaling law associated with a single characteristic length scale.

DOI: 10.1103/PhysRevLett.110.096101 PACS numbers: 81.15.Hi, 46.70.Lk, 68.35.Ct, 81.10.Aj

Self-assembled islands are extensively under scrutiny both for their present and promising applications in electronics or optics and for their insights into the fundamental processes of epitaxial growth. SiGe island formation results from the Stranski-Krastanov mode, where the initial planar growth enforced by wetting leads above a critical height h_c to islands relaxing the elastic strain. As time proceeds, the initially defect-free islands grow, change shape, or eventually dislocate [1]. At low misfit ($\sim 1\%$), this evolution begins with a nucleationless instability [2,3] where periodic ripples basically depicted by the Asaro-Tiller-Grinfeld (ATG) instability allow partial elastic relaxation [4]. The atomic processes at the origin of this evolution differ noticeably from the nucleation pathway at work in the 2D or 3D transition for larger strain [5], so that different growth dynamics and spatial organization may result.

Of special interest is the coarsening of islands where the largest, more relaxed ones grow at the expense of the smallest. The initial isotropic mounds undergo a noninterrupted coarsening different from the standard Ostwald power laws [6,7]. Once the island slopes reach 11°, (105) facets and pyramids appear [2,8–10] whose coarsening is initially enhanced by elasticity [11]. The ripening of the subsequent anisotropic islands was first advocated to reach equilibrium due to the balance between edge, surface, and elastic energies [12,13], while an anomalous coarsening was advocated based on real-time observations showing a reversible shape evolution [14]. In the high-strain nucleation regime, e.g., for pure Ge on Si, coarsening was found to be kinetically suppressed for sparse islands due to a size-dependent nucleation barrier [15] or when supersaturation is high enough [16].

We investigate in this Letter the coarsening in the nucleationless low-strain regime considering the long-time annealing of dense pyramids. We find nearly stationary states with only pyramidal islands whose density depends on the film thickness. We compare the experimental findings with the nonlinear analysis of the surface diffusion equation accounting for wetting, elasticity, and anisotropy in order to rationalize the origin of the coarsening interruption. We find that both the system evolution and morphology can be qualitatively and quantitatively described by the continuum model with parameters extracted from experiments. A mean-field analysis based on these parameters shows that coarsening is interrupted when its driving force vanishes thanks to anisotropy. The theoretical and experimental island size distributions are also found to closely match.

Experimental results and nearly stationary states.—Growth experiments were performed by molecular-beam epitaxy on a Si(100) substrate in a Riber system with a base pressure of 10^{-11} Torr. After a 950 °C *in situ* flashing, a Si 50-nm-thick buffer layer is deposited at 750 °C to provide a clean reproducible flat surface. The Si flux coming from an electron-beam evaporator is constant, 0.03 nm/s, while Ge is deposited from an effusion cell. Si substrates are rotated during growth, and their temperature is controlled in real time. The growth and annealing temperature is 550 °C, and the $Si_{1-x}Ge_x$ composition varies between $x = 0.15$, 0.2, 0.25, 0.3, and 0.5. For the first four compositions, the evolution is nucleationless, while nucleation is clearly visible for $x = 0.5$. In the following, when not specified, the film composition is 0.3. Surface morphologies are analyzed by atomic force microscopy (AFM) in the air tapping mode.

As-grown samples display the ATG instability morphology characterized in real space by a standard deviation $w = 0.2$ nm and in Fourier space by a maximum for a wave vector modulus corresponding to a 130 ± 20-nm wavelength [Fig. 1(a)]. The subsequent *in situ* long-term annealing at the growth temperature induces the development and coarsening of dislocation-free islands above the wetting layer; see Figs. 1(a)–1(d) for a 5-nm-thin epilayer annealed for up to 54 h. To simplify the analysis, we focus on a growth regime with only pyramidal islands [14], contrary to thick films where both pyramids and domes coexist [8]. Initially zero, the island density increases and, after some time, saturates at 2.4×10^{13} m^{-2} in a nearly stationary regime. As checked by AFM profile angle analysis, these islands are bounded by (105) facets and are square or rectangular pyramids. A similar evolution is found for a film thickness $\bar{h} = 8$ nm: The instability displays a similar wavelength and amplitude and leads to a nearly stationary state with an increased density of 2.9×10^{13} m^{-2} [Fig. 1(d)]. Note that the time necessary to reach this state is noticeably decreasing with $\bar{h}$ (it is already achieved after 18 h when $\bar{h} = 8$ nm). We also deposited films of thickness 3.5 and 4.3 nm which did not show any evolution even after 72-h annealing, so that h_c lies in between 4.3 and 5.0 nm for $x = 0.3$. For $x = 0.25$, we found a similar evolution but with (i) a larger h_c, (ii) thicker films up to 20 nm, and (iii) a larger characteristic time. Films with similar thicknesses and $x = 0.15$ and 0.2 did not show any significant evolution, as the characteristic time scale is out of reach.

Continuum model and qualitative comparison.—In order to investigate the origin of these nearly stationary states, we use a continuum model dictated by mass conservation [17,18] which allows us to describe self-organization on large scales. During annealing, the evolution by surface diffusion of the film surface located at $z = h(x, y, t)$ is

$$\frac{\partial h}{\partial t} = D\boldsymbol{\Delta}_s \frac{\delta}{\delta h}(\mathcal{F}^s + \mathcal{F}^{\mathrm{el}}), \tag{1}$$

with the diffusion coefficient D and the surface Laplacian $\boldsymbol{\Delta}_s$. Strain is present in the whole system, as the film-substrate interface is coherent while the two materials have different lattice parameters. The elastic energy $\mathcal{F}^{\mathrm{el}}$ may be computed exactly [18] by solving mechanical equilibrium for small slopes

$$\mathcal{F}^{\mathrm{el}} = \mathcal{E}_0 \int dxdyh\Big[1 + 2(1+\nu)\Big\{-\frac{1}{2}\mathcal{H}_{ii}[h] - |\boldsymbol{\nabla} h|^2 + \mathcal{H}_{ij}[h]\theta_{ijkl}\mathcal{H}_{kl}[h]\Big\}\Big], \quad \text{with}$$

$$\tilde{\mathcal{H}}_{ij}[h](\boldsymbol{k}) = \frac{k_i k_j}{|\boldsymbol{k}|}\tilde{h}(\boldsymbol{k}), \tag{2}$$

with x or y indices, the flat film elastic energy density $\mathcal{E}_0$, the Poisson ratio ν, a geometrical tensor θ_{ijkl}, and the nonlocal operator $\mathcal{H}_{ij}$ defined in Fourier space along x and y with the wave vector $\boldsymbol{k}$. The surface energy $\mathcal{F}^s = \int \gamma dS$ accounts for wetting and crystalline anisotropy. When h is small, the surface energy describing the intermolecular broken bonds depends on the local environment and hence on h [19]. This crucial wetting effect [10] rationalizes the existence of a critical thickness h_c below which the elastic instability cannot occur [19,20]. It also suppresses the singularity of the ATG instability when combined with nonlinear nonlocal effects [6,21]. We consider the exponential dependence for semiconductors [18,19]

$$\gamma_w(h) = \gamma_f(1 + c_w e^{-h/\delta_w}), \tag{3}$$

with the thick film surface energy γ_f, which is consistent with *ab initio* calculations [22,23] and is mainly important at low thickness. In addition, the crystalline anisotropy enforces an extra dependence on the surface slope [24]. The anisotropy of SiGe is such that (100) is stable but not a facet orientation while (105) is a facet [25]. We simplify the analysis of Ref. [18] and consider that $\gamma = \gamma_w(h) + \gamma_{\mathrm{anis}}(\boldsymbol{\nabla} h)$, where

$$\gamma_{\mathrm{anis}} = -\sum_\alpha A_\alpha \exp\Big(-\eta_\alpha\sqrt{|\boldsymbol{\nabla} h - \boldsymbol{\nabla} h_\alpha|^2 + \epsilon_\alpha}\Big), \tag{4}$$

with the (100) and (105) orientations α and a flat minimum for (100) and sharp ones for (105). Its simplicity allows an efficient computation and hence a systematic analysis. In our conditions (low x), the amount of intermixing is expected to be low in contrast to the nucleation regime

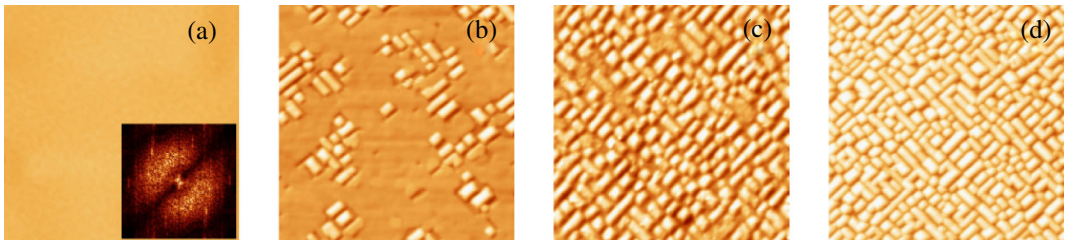

FIG. 1 (color online). AFM images of a 5-nm-thin $Si_{0.70}Ge_{0.30}$ layer (a) as grown (Fourier transform in inset), (b) after 18-h annealing, and (c) after 54-h annealing at 550 °C. (d) Image of a 8-nm film after 18-h annealing. The [110] direction is horizontal. (The scan area is 3×3 μm^2, and the vertical scale is 32 nm.)

(high x) [26], and its effect is hence ignored in a first step. Eventually, we neglect additional effects such as surface stress, alloying, and segregation [7,27,28], but we show below that it suffices to reproduce some experimental results [10,29,30].

The evolution equation (1) was numerically integrated on large time scales using a pseudospectral method [31]. The initial condition is given by the morphology of the instability described by (1) with the same roughness $w = 0.2$ nm as in experiments. The typical surface evolution is depicted in Fig. 2, with the space and time scales $l_0 = \gamma_f/[2(1+\nu)\mathcal{E}_0]$ and $t_0 = l_0^4/(D\gamma_f)$. As time increases, the surface slope increases until it reaches the (105) orientation. At some random locations, some pyramids arise in groups while the instability is still developing in other regions [Fig. 2(b)], which is qualitatively similar to the intermediate experimental morphology in Fig. 1(b). It is worthwhile noting that the coexistence of such regions originates here from the intrinsic randomness of the instability but not from a nucleation process. On larger time, the wetting layer is fully covered and coarsening produces large pyramids [Fig. 2(c)]. Later on, the island density does not significantly evolve and the system reaches a nearly stationary state. Both square and rectangular pyramids are visible, the latter being more numerous for larger thicknesses [Figs. 1(d) and 2(d)].

Quantitative analysis.—The evolution described above is found for different sets of parameters as long as the typical SiGe anisotropy is included with stiff (105) minima and a shallow (100) one. We now turn to a quantitative analysis of the system. First-principles calculations [32] show that the (105) strained orientation displays a surface energy ~1% lower than (100) for a strain corresponding to $x = 0.3$. We enforce this condition together with a moderate stiffness relative to γ_f for the (100) orientation, $\tilde{\gamma}_{100} = 1.4$. We ensure the positiveness of $\tilde{\gamma}$ for the other orientations and consider a shallow minimum for (100) with $\eta_{100} = 10$ and $\epsilon_{100} = 0.01$ and a sharp one for (105) with $\eta_{105} = 20$ and $\epsilon_{105} = 6 \times 10^{-4}$. We checked that these parameters mainly rule the pyramidal shapes but do not alter significantly the island densities. A first crucial parameter is the characteristic length which we set by the instability wavelength. The Fourier transform of the experimental initial corrugation [Fig. 1(a)] displays a maximum for $\lambda_{\mathrm{ATG}} = 130$ nm. It is described by the linear analysis where an $e^{i\boldsymbol{k}\cdot\boldsymbol{r}}$ modulation grows as $e^{\sigma_k t}$ with $\sigma = -\gamma''(\bar{h})/\gamma_f \boldsymbol{k}^2 + |\boldsymbol{k}|^3 - \tilde{\gamma}_{100}\boldsymbol{k}^4$. This growth rate is maximum for a given $k_{\max}$ that we set equal to $2\pi/\lambda_{\mathrm{ATG}}$, which leads to the length scale $l_0 \simeq 13$ nm. This result is typical of an experimental mean Ge concentration, which has small fluctuations due to segregation and intermixing. These fluctuations should slightly renormalize the instability wavelength [27], but the adjusting procedure allows us to consider this effect as second order.

Wetting also significantly impacts the quantitative results. It is a function here of c_w and δ_w. We fit the decay given by first-principles calculations of $\gamma(h)$ for a strained film with different surface reconstructions [23] and find $\delta_w = 1.8$ monolayers, which is 0.075 in dimensionless units. The critical height associated with an exponential wetting potential (consistent with *ab initio* calculations done for up to 5 monolayers [23]) is $h_c = \delta_w \log(4\tilde{\gamma}_{100} c_w/\delta_w^2)$. Experimentally, we found that h_c lies in between 4.3 and 5.0 nm. The relatively long time for the instability to arise when $\bar{h} = 5.0$ nm suggests that h_c is in the vicinity of this thickness. Eventually, we find a good comparison between theory and experiments using $h_c = 0.37$ (4.8 nm), which gives $c_w = 0.14$.

The results of the continuum model are confronted to experiments in Fig. 3 where we plot the island density in the nearly stationary state ρ_{fin} as a function of $\bar{h}$. No islands are found below h_c when wetting enforces a stable strained film. Above h_c, the island density increases with $\bar{h}$ as more matter is available to fill more islands. The density given by the model is 97% of the experiments for the 5- and 8-nm films, while the measured and predicted densities both increase by 20%. The overall agreement is satisfactory, and we argue that the experiments are well described on large scales by such a nucleationless interrupted coarsening.

Mean-field energy landscape.—To rationalize the origin of this interruption, we turn to a mean-field description of the ripening kinetics. In order to describe the mass transfer between objects, the analysis of Ref. [33] was extended in Ref. [18] by considering the coarsening of two islands.

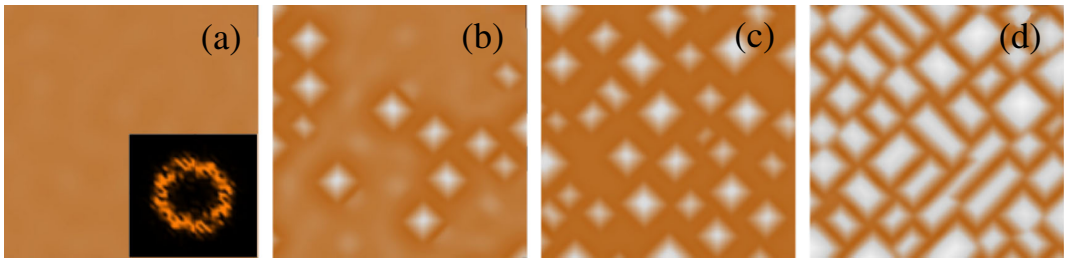

FIG. 2 (color online). Numerical resolution of the diffusion equation (1) for a strained anisotropic film for (a) a 5-nm film and $t = 0$ (Fourier transform in inset), (b) 18 h ($240t_0$), (c) 54 h ($720t_0$), and (d) an 8-nm film and $t = 18$ h ($240t_0$). [The scan area is 1.2×1.2 μm^2($= \sqrt{2}64l_0$), and the vertical scale is 31 nm.]

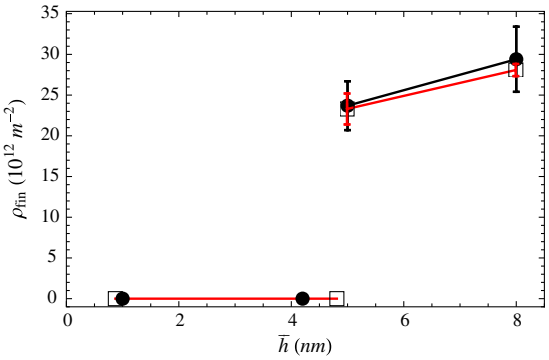

FIG. 3 (color online). Island density in the nearly stationary state as a function of the film thickness in experiments (black line and dots) and theory (red line and squares).

We implement this analysis with the parameters found above to find the characteristic time scale for coarsening. We consider pyramidal islands on a wetting layer, with different volumes V_1 and V_2 separated by d. The pyramidal shape is crucial, as it implies that the relaxation energy is merely proportional to V, while a larger relaxation which would occur by changing the island shape is not considered. The formation energy is the sum for both islands of Ref. [18],

$$\Delta E = \hat{\gamma} V^{2/3} - \lambda^{\rm el} V + \hat{c}_w [V_w^{2/3} - V^{2/3}](e^{V/\delta_w d^2} - 1). \quad (5)$$

The first term stands for the surface energy, and the second one stands for the elastic relaxation. The last wetting term describes the fact that, if matter goes from the wetting layer to the islands, the former becomes thinner and hence has a larger surface energy.

We consider numerical values appropriate for our systems: The pyramids are made of (105) facets, the film thickness is 8 nm, and d is computed from the island density. We use the parameters c_w and δ_w found above and, similarly, a (105) surface energy 1% lower than (100). The energy ΔE as a function of the dimensionless volumes is plotted in Fig. 4. At low volume, ΔE mainly decreases due to the elastic $-V$ relaxation but it raises steeply for larger volumes, as the wetting layer is peeled due to mass conservation. Separating these behaviors, a line of troughs (black line) is bent downward so that the strict energy minima correspond to a full coarsening where either V_1 or V_2 vanishes. However, different islands may coexist in the valley of this energy landscape. The maximal difference in energy per atom in this valley is $\Delta\mu \simeq 4 \times 10^{-5}$ eV, and the typical chemical potential gradient is $\nabla\mu \simeq \Delta\mu/d$. The surface diffusion flux is $J_s = -D_s \nabla\mu / a^2 k_B T$, with the lattice parameter a and the diffusion coefficient D_s. The diffusion coefficient is related to t_0 [34], which may be found from our experiments by fitting the time where the theoretical morphology, Fig. 2(b) at $t = 240 t_0$, resembles the AFM image, Fig. 1(b) at $t = 18$ h, with the result $t_0 = 270$ s. This value is 10 times larger than the value which would result from a surface diffusion barrier of 1.4 eV computed for strained Ge [35]. Considering the mass conservation equation $|dV_1/dt| = a^3 L_1 J_s$ with the island width L_1, the time scale for such a low chemical potential gradient is $\simeq 8500$ h for the coarsening of two islands, well above the experimental time scale. This rationalizes a nucleationless interrupted coarsening by the vanishing of the driving force for mass transfer. Note that this result applies only with a single island shape and not when different shapes coexist, as seen in experiments for a larger thickness [36].

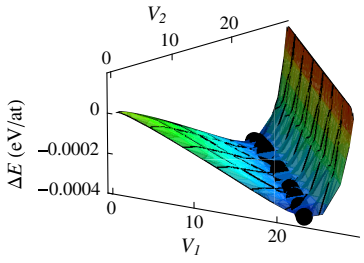

FIG. 4 (color online). Energy of two islands as a function of their volumes following the mean-field calculation (5). The black line underlines the curvature of the trough.

Size distribution.—We turn to the size distribution of the resulting islands. For a submonolayer growth with a deposited coverage Θ, the number N_s of islands with s atoms is expected to follow the scaling form [37]

$$N_s = \frac{\Theta}{\langle s \rangle^2} f\left(\frac{s}{\langle s \rangle}\right), \quad (6)$$

in the absence of any characteristic length besides the mean island size $\langle s \rangle$. It is not modified by elastic interactions for submonolayer islands [38], while it may be extended to 3D objects by considering the volume distribution and Θ as the coverage beyond the 2D-3D transition [39]. We checked the validity of the scaling form both in experiments and theory; see Fig. 5. It is significant, as the system results here from an

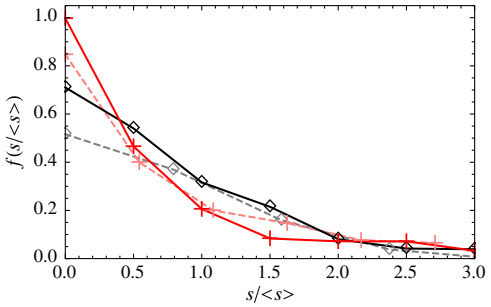

FIG. 5 (color online). Rescaled island size distribution following Eq. (6), with the island volume s, mean volume $\langle s \rangle$, and coverage above the wetting layer Θ. The solid black (open diamond) and red (plusses) lines correspond to the experiments for the 5- and 8-nm films. The dashed gray (open diamond) and pink (plusses) lines correspond to the model for these thicknesses.

instability with a characteristic wavelength λ_{ATG}. The scaling law is therefore at work both in the aggregation-diffusion nucleation [39] *and* instability regimes even if they involve different microscopic mechanisms. Moreover, the experimental and theoretical scaling functions are relatively similar, displaying a monotonic decrease and a noticeable dispersion, showing again the relevance of the continuum description.

As a conclusion, a joint experimental and theoretical study gives a quantitative description of the self-assembly of strained SiGe pyramids. We find that, in the low-strain regime after the onset of the ATG-like instability, the long-time dynamics leads to nearly stationary states where the island density depends on the mean film height. The experimental outcomes are described by a nonlinear analysis of the diffusion equation describing self-organization on large scales and including wetting, elastic relaxation, and an anisotropic surface energy. The interrupted evolution is ascribed by the vanishing of the coarsening driving force when islands display similar shapes and low chemical potential differences. We suggest that this self-organization dynamics is generic and could describe other systems, e.g., III–V low strained quantum dots with a single island shape. These results call for further study of the influence of wetting on the self-organization dynamics, e.g., by using surfactant. The combination of the morphological evolution with additional effects such as alloying would also be of practical and fundamental interest.

*aqua@insp.jussieu.fr
†isabelle.berbezier@im2np.fr

[1] J. N. Aqua, I. Berbezier, L. Favre, T. Frisch, and A. Ronda, Phys. Rep. **522**, 59 (2013).
[2] P. Sutter and M. G. Lagally, Phys. Rev. Lett. **84**, 4637 (2000).
[3] R. M. Tromp, F. M. Ross, and M. C. Reuter, Phys. Rev. Lett. **84**, 4641 (2000).
[4] R. J. Asaro and W. A. Tiller, Metall. Trans. **3**, 1789 (1972); M. A. Grinfeld, Sov. Phys. Dokl. **31**, 831 (1986).
[5] C.-H. Lam, C.-K. Lee, and L. M. Sander, Phys. Rev. Lett. **89**, 216102 (2002).
[6] J.-N. Aqua, T. Frisch, and A. Verga, Phys. Rev. B **76**, 165319 (2007).
[7] M. S. Levine, A. A. Golovin, S. H. Davis, and P. W. Voorhees, Phys. Rev. B **75**, 205312 (2007).
[8] J. Stangl, V. Holý, and G. Bauer, Rev. Mod. Phys. **76**, 725 (2004).
[9] I. Berbezier and A. Ronda, Surf. Sci. Rep. **64**, 47 (2009).
[10] M. Brehm *et al.*, Phys. Rev. B **80**, 205321 (2009).
[11] J. A. Floro, M. Sinclair, E. Chason, L. Freund, R. Twesten, R. Hwang, and G. Lucadamo, Phys. Rev. Lett. **84**, 701 (2000).
[12] V. A. Shchukin and D. Bimberg, Rev. Mod. Phys. **71**, 1125 (1999).
[13] G. Medeiros-Ribeiro, A. M. Bratkovski, T. I. Kamins, D. A. A. Ohlberg, R. S. Williams, Science **279**, 353 (1998).
[14] A. Rastelli, M. Stoffel, J. Tersoff, G. S. Kar, and O. G. Schmidt, Phys. Rev. Lett. **95**, 026103 (2005); F. M. Ross, J. Tersoff, and R. M. Tromp, Phys. Rev. Lett. **80**, 984 (1998).
[15] B. Voigtänder, Surf. Sci. Rep. **43**, 127 (2001).
[16] M. R. McKay, J. A. Venables, and J. Drucker, Phys. Rev. Lett. **101**, 216104 (2008).
[17] B. J. Spencer, P. W. Voorhees, and S. H. Davis, Phys. Rev. Lett. **67**, 3696 (1991).
[18] J.-N. Aqua and T. Frisch, Phys. Rev. B **82**, 085322 (2010).
[19] See, e.g., P. Müller and R. Kern, Appl. Surf. Sci. **102**, 6 (1996); C.-H. Chiu and H. Gao, in *Thin Films: Stresses and Mechanical Properties V*, edited by S. P. Baker *et al.*, MRS Symposia Proceedings No. 356 (Materials Research Society, Pittsburgh, 1995), p. 33.
[20] J. Tersoff, Phys. Rev. B **43**, 9377 (1991).
[21] See, e.g., W. H. Yang and D. J. Srolovitz, Phys. Rev. Lett. **71**, 1593 (1993); A. A. Golovin, S. H. Davis, and P. W. Voorhees, Phys. Rev. E **68**, 056203 (2003).
[22] M. J. Beck, A. van de Walle, and M. Asta, Phys. Rev. B **70**, 205337 (2004).
[23] G.-H. Lu and F. Liu, Phys. Rev. Lett. **94**, 176103 (2005).
[24] G. Wulff, Z. Kristallogr. **34**, 449 (1901); P. Nozières, in *Solids Far from Equilibrium*, edited by C. Godrèche (Cambdrige University Press, Cambridge, England, 1991), p. 1.
[25] J. Tersoff, B. J. Spencer, A. Rastelli, and H. von Känel, Phys. Rev. Lett. **89**, 196104 (2002).
[26] See, e.g., P. Castrillo, R. Pinacho, M. Jaraiz, and J. E. Rubio, J. Appl. Phys. **109**, 103502 (2011).
[27] B. J. Spencer, P. W. Voorhees, and J. Tersoff, Phys. Rev. B **64**, 235318 (2001).
[28] Y. Tu and J. Tersoff, Phys. Rev. Lett. **93**, 216101 (2004).
[29] J. J. Zhang *et al.*, Phys. Rev. Lett. **109**, 085502 (2012).
[30] H. Hu, H. Gao, and F. Liu, Phys. Rev. Lett. **109**, 106103 (2012).
[31] A.-K. Kassam and L. N. Trefethen, SIAM J. Sci. Comput. **26**, 1214 (2005).
[32] O. E. Shklyaev, M. J. Beck, M. Asta, M. J. Miksis, and P. W. Voorhees, Phys. Rev. Lett. **94**, 176102 (2005).
[33] L. G. Wang, P. Kratzer, M. Scheffler, and N. Moll, Phys. Rev. Lett. **82**, 4042 (1999).
[34] $D = l_0^4/(t_0\gamma_f)$, while $D_s = Dk_BT/a^4$.
[35] E. Bussmann and B. S. Swartzentruber, Phys. Rev. Lett. **104**, 126101 (2010).
[36] The continuum model for thick films gives new larger islands that are rather isotropic.
[37] M. C. Bartelt and J. W. Evans, Phys. Rev. B **46**, 12 675 (1992).
[38] J.-N. Aqua and T. Frisch, Phys. Rev. B **78**, 121305(R) (2008).
[39] T. J. Krzyzewski, P. B. Joyce, G. R. Bell, and T. S. Jones, Phys. Rev. B **66**, 201302 (2002).